ACS Photonics

pubs.acs.org/journal/apchd5

Article

Experimental Demonstration of Light-Trapping Transparent Electrode Geometries

Mengdi Sun, Pooria Golvari, Stephen Michael Kuebler, and Pieter G. Kik*

Cite This: https://doi.org/10.1021/acsphotonics.2c01468

Read Online

ACCESS | Metrics & More | Article Recommendations | Supporting Information

ABSTRACT: The intrinsic trade-off between conductivity and transparency has long impeded the development of truly transparent electrodes. Recently, a transparent electrode design was introduced that promised remarkably high electrical conductivity while allowing near-complete transmission of incident light into the underlying optical device. The approach is based on the use of metallic wires with inclined surfaces, embedded in a transparent dielectric film. Light reflected by metallic regions of the sample can be recovered by total internal reflection, resulting in efficient trapping of light incident on conductive regions. Prototype electrode geometries were fabricated by multiphoton lithography and selective chemical deposition. Light trapping is observed by optical microscopy and laser scanning experiments for surface tilt angles exceeding 25°. Approximately 60% of light reflected by the metallic electrode surface was recovered through total internal reflection. The presented approach could lead to optoelectronic devices with significantly improved performance across a wide spectral bandwidth.

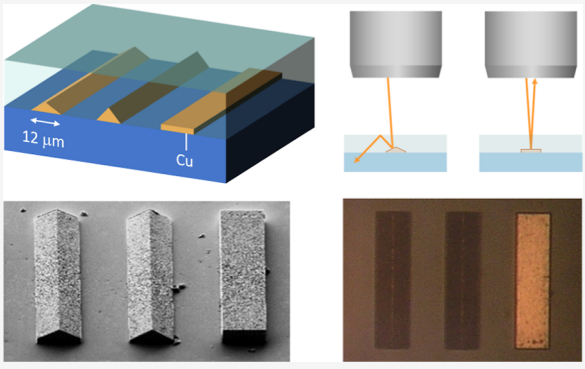

KEYWORDS: *light trapping, transparent electrodes, multiphoton lithography, selective chemical deposition*

INTRODUCTION

Transparent electrodes have a wide range of applications in optoelectronic devices, including high-speed photodetectors, photovoltaic solar cells, and smart displays.[1−12] To achieve high device performance, both high optical transparency and large electrical conductivity are required. For wire-based electrodes, one of the major sources of optical loss is back-reflection by metallic contacts, which is typically reduced by using low metal areal coverage. However, lowering the metal coverage results in increased resistive losses and longer charge carrier collection paths. A variety of techniques have been studied to achieve simultaneous high transparency and high conductivity, including encapsulated front contacts,[13−16] high-aspect-ratio metallic electrodes,[17−20] and graded-index nanostructures,[21−24] each with their own advantages and drawbacks in performance and manufacturing complexity. State-of-the-art transparent electrodes have achieved >90% optical transmittance and <10 Ω/sq sheet resistance, including the designs reported by Saive et al.[20] (T = 99.86% and R_{sh} = 4.8 Ω/sq), Hsu et al.[25] (T = 92% and R_{sh} = 0.36 Ω/sq), and van de Groep et al.[8] (T = 91% and R_{sh} = 6.5 Ω/sq).

A novel type of transparent electrode that uses light trapping to mitigate the shadowing losses has been proposed,[26] schematically shown in Figure 1a. In this design, metallic front contacts with tilted surfaces are embedded in a dielectric cover layer. The tilt angle of the electrode is selected such that light incident on the electrode surface is reflected toward an angle larger than the critical angle between the encapsulation layer and the external medium. Under these conditions, the redirected light undergoes total internal reflection (TIR) at the top surface of the cover layer, virtually eliminating all shadowing losses. The optical and electrical performance of such electrodes has been investigated in detail numerically,[27,28] and a remarkably low effective sheet resistance of R_{sh} = 0.35 Ω/sq at 97% transparency was reported for 2 μm wide silver wires, with lower sheet resistance values and higher transparency predicted for larger wire sizes at the same areal coverage. Note that the structure shown in Figure 1a shares superficial similarities with a previously investigated transparent electrode design by Saive et al.[20] However, that prior approach relied on enhanced forward scattering by high-aspect-ratio structures, whereas the structure discussed here relies on low-aspect-ratio structures that produce back-reflection followed by TIR. The latter represents a fundamentally different approach that potentially enables more mechanically robust devices. Figure 1b shows an example of the electric-field distribution around a triangular metallic

Received: September 19, 2022

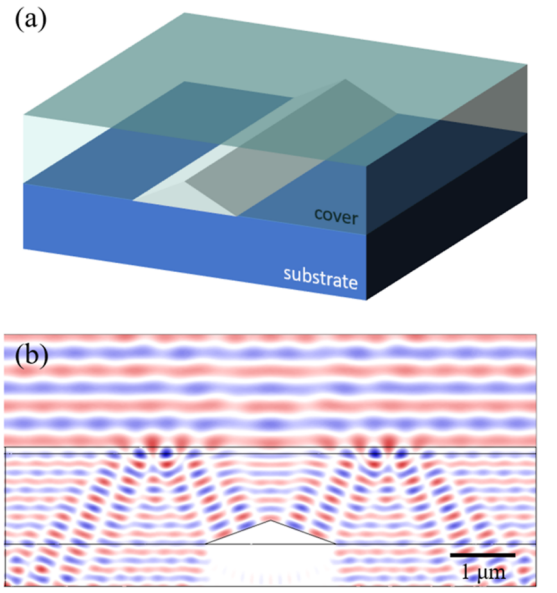

Figure 1. (a) Schematic of a triangular light-trapping transparent electrode and (b) numerically simulated instantaneous E-field distribution around a light-trapping electrode with 20° surface tilt, under 600 nm normal-incidence TE illumination.

wire with a wire width of 2 μm and a surface tilt of 20°, embedded in a cover layer with a refractive index of $n = 2$ corresponding to a critical angle of $\theta_c = 30°$. The field distribution was simulated using CST Studio[29] using literature values for the silver dielectric function to represent the metallic wires.[30] Normal incidence illumination with 600 nm light is seen to produce TIR of light reflected by the metallic wire, demonstrating efficient light trapping. Simulations indicate that this design could provide high conductivity and dramatically reduced shadowing losses over a wide angular range and across a broad spectral range. Here, we present the first experimental demonstration and optical characterization of this light-trapping design.

RESULTS AND DISCUSSION

To demonstrate the concept of light trapping by inclined metallic electrodes, proof-of-concept electrode geometries were fabricated using multiphoton lithography (MPL) and subsequently metallized by electroless deposition (see the Methods section). MPL enables prototyping of arbitrary wire geometries, while the electroless metal deposition ensures that the outer surface of the fabricated wires has optical properties that approach those of solid metal wires, in turn enabling detailed analysis of the optical performance. The metallization process used in this work is based on seeded electroless copper deposition[31−33] which yields copper coatings of tunable thickness that are electrically conductive[34−37] and optically reflective.[33] Figure 2 schematically depicts the fabrication workflow. Prototype electrode geometry preforms were patterned in the cross-linkable photopolymer IP-Dip (Nanoscribe) using a home-built MPL system.[38] The preforms were then metallized with copper following a modified literature procedure,[32,33,39] as described in the Methods section. To characterize the light-trapping performance, a drop of index-matching liquid is placed on the sample and a microscope cover slip is added on top, representative of a homogeneous cover layer.

Several electrode geometries were fabricated on the same sample to enable direct performance comparisons. Figure 3a schematically shows the sample design. An array of wires with a length of 50 μm and a width of 12 μm was fabricated. The leftmost and rightmost wires have zero surface tilt (flat wires), while the surface tilt of the remaining six wires is varied from 10 to 35° in steps of 5° from left to right. All wires have a fixed height of 4.5 μm and a relatively small center-to-center spacing of 14 μm to facilitate optical analysis. Figure 3b shows a scanning electron microscopy (SEM) image of the as-fabricated polymeric wires on a glass substrate. Note that the design geometry is well-replicated in the developed polymer. Next, the surface of the wires was selectively metallized via electroless copper deposition. The conformal chemical deposition used in this work enables arbitrary spacing between the wires, in contrast to oblique angle deposition methods which are based on shadowing.[40,41] Figure 3c shows a SEM

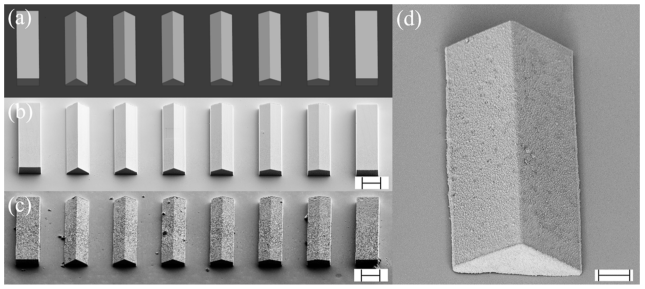

Figure 3. Prototype light-trapping electrode geometries with surface angles ranging from 10 to 35°. (a) Model design and (b) SEM image of the fabricated sample before and (c) after metallization. (d) High-magnification view of a single 20 μm-wide wire with a 30° surface tilt. Scale bars are 10 (a−c) and 5 μm (d).

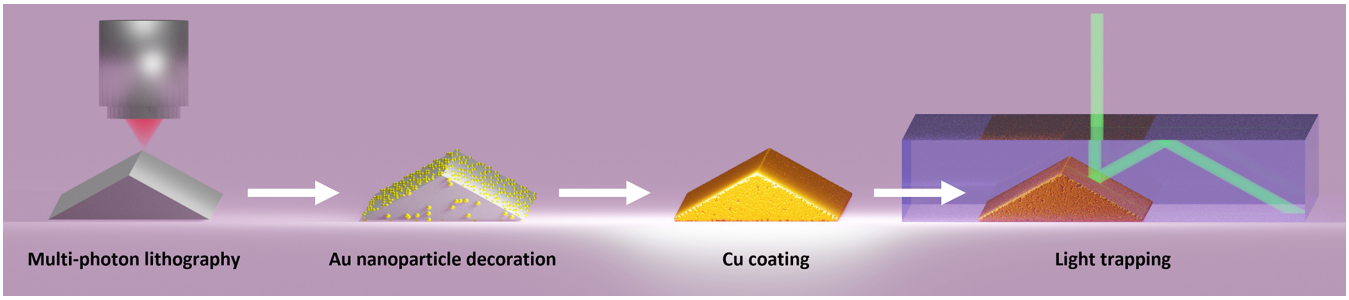

Figure 2. Schematic workflow of the prototype light-trapping electrode geometry fabrication and operation. Preforms are generated via MPL, followed by a two-step metallization. Finally, the light-trapping performance is characterized in laser scanning experiments.

https://doi.org/10.1021/acsphotonics.2c01468
ACS Photonics XXXX, XXX, XXX−XXX

image of the metallized wires. Note that the metallization process does not affect the wire geometry (size, shape, and tilt angle). A magnified perspective view of a representative single wire (Figure 3d) demonstrates the selectivity of the deposition: the surface of the metallized wires reveals a grainy structure due to the morphology of deposited copper nanoparticles,[33] whereas the glass surface remains smooth after metallization. Energy-dispersive X-ray spectroscopy (EDS) measurements confirmed the selective deposition of copper on the fabricated wires (Figure S1 in the Supporting Information).

The optical performance of the light-trapping structures was investigated using optical microscopy. Figure 4a shows a bright-field reflection microscopy image of an as-fabricated array of metallized wires, as well as a schematic of the measurement geometry. An objective lens with 50× magnification and a numerical aperture of NA = 0.8 was used, corresponding to a maximum collection angle of 53°. Illumination was carried out with a small aperture stop, ensuring near-normal illumination spanning a small angular range from −15 to 15°. Metallized wires with tilt angles from 0 to 20° appear bright in reflection mode microscopy because the reflected light lies within the numerical aperture of the objective, as schematically indicated by the leftmost two schematics. Wires with tilt angles greater than 25° gradually become dark because the incident light is redirected toward angles that exceed the numerical aperture of the objective, as indicated in the rightmost schematic. The area surrounding the wires appears relatively dark due to the low reflectance of the glass substrate. Note that the brightness of each wire shows some spatial variation, which is attributed to the surface roughness resulting from the metal deposition process, as observed in Figure 3d.

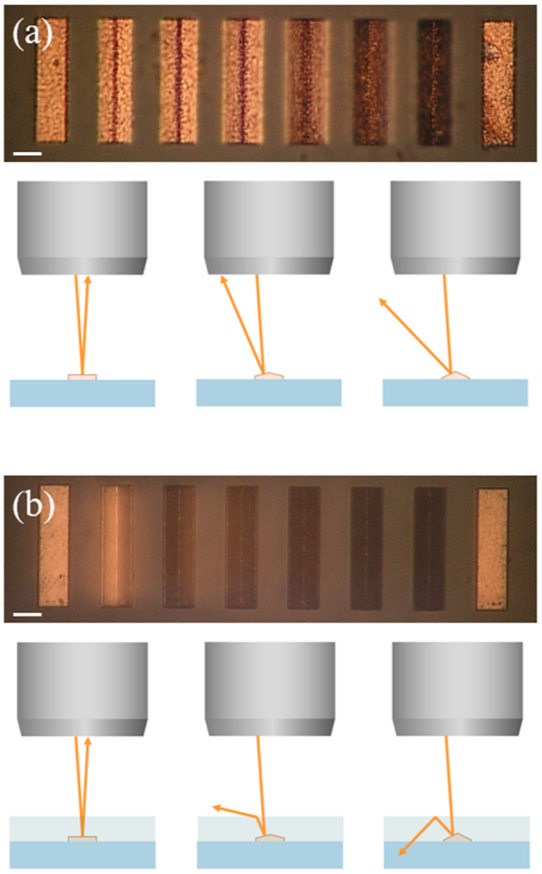

Figure 4. Reflection microscopy image and measurement schematic of (a) uncovered metallized and (b) covered metallized light-trapping structures. The scale bars correspond to 12 μm.

To evaluate the light-trapping performance enabled by the different wire geometries, a drop of index-matching liquid (n = 1.518) was placed on the sample and a microscope cover slip was placed on top. The cover slip and index-matching liquid together take the role of a homogeneous cover layer with a critical angle of θ_c = 41.2°. Under normal incidence illumination, light trapping is therefore expected for wires with a surface tilt exceeding 20.6° corresponding to the three rightmost tilted wires in Figure 3. Figure 4b shows the bright-field reflection image and a measurement schematic of the sample in the light-trapping configuration. In the light-trapping measurement geometry, the leftmost and rightmost wires with 0° tilt still appear bright due to a lack of light trapping, as indicated in the leftmost schematic. The brightness of the wire images decreases significantly for wires with high surface tilt. The third (15° tilt) and fourth (20° tilt) wires already show reduced brightness, despite the fact that the internal reflected angles at normal incidence illumination of 30 and 40°, respectively, are smaller than the critical angle (θ_c = 41.2°). This observation is attributed to the fact that the upward reflected light strongly refracts at the sample surface, leading to angles that are close to or larger than the maximum collection angle of the microscope objective, as shown in the middle schematic. Assuming perfect normal incidence illumination, surface angles of 15 and 20° would produce external angles of 49 and 75°, compared to a maximum collection angle of 53°. Taking into account the nonzero beam spread (approximately 30° angular spread about the normal), a significant fraction of refracted light is not collected, even for the wire with 15° surface tilt, resulting in a dark appearance. The fifth (25° tilt), sixth (30° tilt), and seventh (35° tilt) wires appear largely dark, which is attributed to successful trapping of reflected light, as shown in the rightmost schematic. This analysis suggests that light with an angular spread of ∼30° centered around the surface normal can be trapped efficiently by these structures. Prior theoretical work[28] indicates that the trapping efficiency drops below 50% for illumination angles beyond ∼22° due to loss of TIR. In that work, the use of a higher-index cover layer was found to enable efficient light trapping over a larger angular range, providing a route toward improved angular response. Note that the colorless dark (i.e., approximately black) appearance of the wires with the steepest surface inclination under white-light illumination suggests that light trapping remains efficient across the visible spectrum, consistent with the predictions of spectral performance made in ref 27. The edges of the structure remain visible in the image because sharp edges scatter light into a wide range of angles, some of which will appear below the critical angle, contributing to the image formation. Furthermore, the surface roughness of the wires appears reduced for the covered sample, which is attributed to a reduction in image quality due to the additional refraction introduced on the cover slip surface.

The reduction in the amount of reflected light collected from the sample in bright-field reflection microscopy images in Figure 4 strongly suggests light trapping; however, the trapped light itself was not directly collected. This could lead to an overestimation of the light-trapping performance, as any light exiting the top surface at angles beyond the maximum collection angle of the objective would not be visualized but

https://doi.org/10.1021/acsphotonics.2c01468
ACS Photonics XXXX, XXX, XXX−XXX

would still constitute shadowing losses. To eliminate this source of uncertainty, the light-trapping efficiency was directly measured by collecting the on-axis and off-axis transmitted optical power under normal-incidence laser illumination of individual metallized wires. A sample containing well-separated wires with a length of 100 μm, a width of 20 μm, a height of 5.8 μm, and a surface tilt of 30° (as shown in Figure 3d) with index-matching oil and cover slip applied was placed on top of a prism. In order to enable the collection of trapped light, index-matching oil was applied between the sample and the prism, enabling trapped light to transmit into the prism and subsequently escape through the inclined sides of the dove prism. A moderately focused laser beam (spot size ~20 μm, wavelength 532 nm, TM-polarized) was directed toward the sample at normal incidence, and the position of the entire assembly was scanned such that the wire crossed the laser focus. Optical power detectors were placed both on-axis (angle ~ 0°) and off-axis at an angle close to 60°.

Figure 5 shows the position-dependent power collected by the on-axis detector and the two off-axis detectors, as well as a measurement schematic. All data are normalized to the power transmitted when light is not incident on the wires. As the laser spot moves across the wires, the fraction of power transmitted on-axis (green line) gradually decreases, reaches a minimum of 24%, and then gradually recovers. Note that while the metallized wire is opaque, the laser spot is slightly larger than the wire width, allowing a transmission of 24% even when the spot is centered on the wire. As the on-axis transmission reduces, the off-axis collected powers on the left detector (red line) and right detector (blue line) both increase, demonstrating that a part of the reduction in on-axis transmission is accompanied by trapping and recovery of reflected light. The calculated full-width at half-maximum (fwhm) of all three curves is ~20 μm, similar to the width of the metallized wires and the laser spot. The maximum collected power for the off-axis detectors occurs at slightly different sample positions, as expected due to the fact that the left and right wire facet centers are separated by 10 μm. The two off-axis detectors register a slightly different maximum signal, which might be due to a difference in surface quality of the metallic coating. Similar measurements on a flat reference electrode geometry (not shown) did not reveal any detectable power on the off-axis detectors. Theoretical predictions of the on-axis (dashed green line) and off-axis collected signal in the left and right detectors (dashed red and blue lines, respectively) are included. The calculations consider an incident Gaussian beam with a fwhm of 20 μm. Light incident on the 20 μm wide wire is assumed to be removed from the center detector signal. Of the light incident on the individual 10 μm wide inclined facets of the wire, 55% is assumed to be absorbed by the copper surface, based on literature values for the dielectric function,[30] the incident angle, and the polarization of the light. The remaining light is assumed to be trapped and collected with 100% efficiency. The calculated and experimental curves for off-axis detection show reasonable agreement in width and position, but they differ in magnitude. The experimentally observed signals are likely affected by a combination of diffraction due to the small width of the wires and by scattering from surface imperfections, resulting in non-ideal collection of trapped light by the off-axis optical power meters.

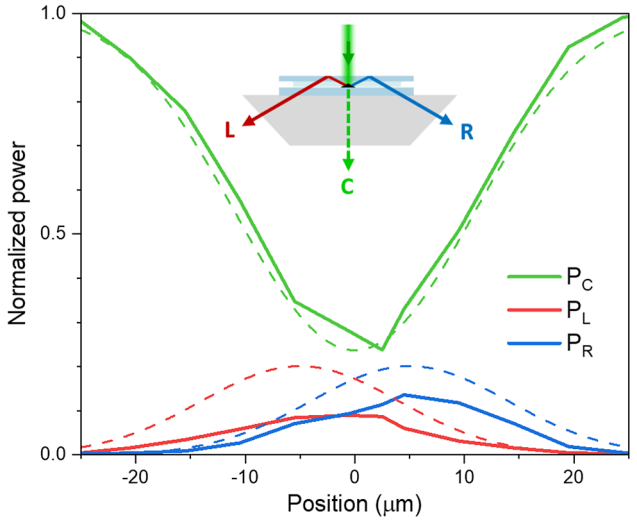

Figure 5. Measured transmitted (P_c) and recovered (P_L, P_R) power (solid lines) obtained from an individual light-trapping wire as a function of position under focused illumination, as well as the corresponding predicted values (dashed lines). The measurement schematic shows the location of the left (L), center (C), and right (R) power detectors.

Based on the position-dependent power curves in Figure 5, the light-trapping efficiency was estimated, defined as the fraction of off-axis power collected relative to the on-axis shadowing losses. From the measurements (solid lines), an average light-trapping efficiency of ~26.5% is found, that is, 26.5% of light that would normally be lost to reflection is recovered through TIR. Taking into account the previously mentioned Cu reflection losses, it is estimated that 59% of light initially reflected by the metallized wire surface is recovered. As stated previously, this value may underestimate the actual trapping efficiency as it does not take into account reduced collection efficiency due to scattering and diffractive effects. The light-trapping efficiency can be further improved by replacing Cu with more reflective metals, such as silver, while the sheet resistance can be reduced by replacing the MPL-written wire cores with metal. For example, the wire geometry with 30° surface tilt would produce an effective sheet resistance R_{sh} of 0.069 Ω/sq for solid Cu[34] wires and 0.055 Ω/sq for solid Ag[30] wires, both at an assumed areal fill fraction of f = 10%. Given the measured light-trapping efficiency, a Cu wire electrode with f = 10% would exhibit an optical transmission of T = 93%, which could be improved substantially by switching to a more reflective metal such as silver. The calculated values for solid copper wires (T = 93% and R_{sh} = 0.069 Ω/sq) are competitive with state-of-the-art light-trapping electrodes and offer important advantages for manufacturability. The presented light-trapping electrode structures have a low surface tilt angle, which is expected to produce relatively robust wires compared with the high-aspect-ratio structures reported by Saive et al.[20] The grating-based design by van de Groep et al.[8] achieves 91% transmission at 6.5 Ω/sq; however, this approach requires nanopatterning and shows strong polarization and spectral dependence. In contrast, the light-trapping approach presented here allows broadband use with relatively low polarization dependence, as demonstrated in ref 27.

CONCLUSIONS

In conclusion, we have experimentally demonstrated a novel light-trapping transparent electrode geometry. Prototype

https://doi.org/10.1021/acsphotonics.2c01468
ACS Photonics XXXX, XXX, XXX−XXX

samples were fabricated using MPL and selective chemical deposition. The light-trapping process was demonstrated experimentally using optical microscopy and spatially resolved transmission measurements. The experiments indicate that at least 59% of light reflected by copper-coated wires with a surface tilt of 30° is recovered through TIR. The demonstrated design and related structures could dramatically reduce shadowing losses in a wide range of optoelectronic devices across a wide spectral range spanning from the ultraviolet to the far infrared.

METHODS

Sample Fabrication. Prototype electrode geometries were fabricated on a glass substrate using a home-built MPL system described elsewhere.[38] In brief, the output of a femtosecond mode-locked Ti:sapphire laser was focused through a high-N.A. objective lens into a commercial acrylic resin, IP-Dip (Nanoscribe), to induce multiphoton polymerization. Using a three-axis nanopositioner, the focal volume was controllably positioned with respect to the substrate to define the 3D pattern. The exposed 3D volume determines the shape of the eventual prototype electrode geometries. The unpolymerized resin was washed three times with propylene glycol monomethyl ether acetate to develop the microstructure, rinsed twice with isopropanol, and allowed to dry in air. The fabricated structures were metallized through selective deposition using a modified literature procedure.[32,33,39] The polymeric microstructures were washed with *N*,*N*-dimethyl-formamide and immersed in an ethanoic solution of ethylene diamine (20 vol %) for 2 h. Amines react selectively with the unreacted acrylic groups of the polymer through Michael addition, leaving behind pendant amine groups on the surface. The sample was washed thoroughly with ethanol and DI water. The substrate was then immersed in tetrachloroauric acid (0.53 mM in DI water) for 2 h to immobilize Au^{3+} ions by coordination to the aminated surface, then washed with DI water, and immersed in a solution of sodium borohydride (0.1 M in water) to form surface-bound AuNPs.[42] Importantly, the substrate was then rinsed with dilute HNO_3 (1 wt % in water) to wash away any unbound AuNPs. The AuNP-primed surface was used for electroless copper enhancement to create reflective surfaces on the 3D written wires. A bath of Cu^{2+} (copper sulfate 1.5 wt %, sodium hydroxide 2 wt %, and sodium potassium tartrate 7 wt % in DI water) was prepared. To 5 mL of the filtered solution, 0.5 mL of aqueous formaldehyde (37 wt %) was added under vigorous stirring. The substrate was immersed in the activated bath for 10 min and washed with copious DI water. The immersion in the copper bath and the subsequent water rinse were repeated two more times to yield a reflective layer on the wires.

Optical Characterization. Optical microscopy images were taken in an Olympus BX51TRF microscope in the bright-field reflection mode under the illumination of unpolarized white light. Images of light-trapping samples were taken by placing index-matching oil (Cargille non-drying immersion oil for microscopy, $n = 1.518$) between the sample and a #1.5 cover slip (thickness 170 μm). Spatially resolved transmission measurements were carried out using a 532 nm diode-pumped solid-state laser with an optical power of ~1 mW. The beam width was reduced from 0.6 mm to 20 μm using a two-lens system with $f_1 = 5$ cm, $f_2 = 10$ cm, and a lens separation of 75 cm. The prototype electrode geometries were illuminated with TM polarized light (electric field parallel to the long axis of the wire). The transmitted power was measured using a Newport 918D-SL-OD3R silicon photodetector.

ASSOCIATED CONTENT

Supporting Information

The Supporting Information is available free of charge at https://pubs.acs.org/doi/10.1021/acsphotonics.2c01468.

Details of the energy dispersive X-ray spectroscopy of the fabricated prototype electrode geometries (PDF)

AUTHOR INFORMATION

Corresponding Author

Pieter G. Kik − *CREOL, The College of Optics and Photonics, University of Central Florida, Orlando, Florida 32816, United States; Physics Department, University of Central Florida, Orlando, Florida 32816, United States;* orcid.org/0000-0003-3575-3865; Email: kik@creol.ucf.edu

Authors

Mengdi Sun − *CREOL, The College of Optics and Photonics, University of Central Florida, Orlando, Florida 32816, United States;* orcid.org/0000-0001-5031-0443

Pooria Golvari − *Chemistry Department, University of Central Florida, Orlando, Florida 32816, United States;* orcid.org/0000-0001-6369-006X

Stephen Michael Kuebler − *CREOL, The College of Optics and Photonics, University of Central Florida, Orlando, Florida 32816, United States; Chemistry Department and Department of Material Science and Engineering, University of Central Florida, Orlando, Florida 32816, United States*

Complete contact information is available at: https://pubs.acs.org/10.1021/acsphotonics.2c01468

Author Contributions

M.S. and P.G. contributed equally to this work. The manuscript was written through contributions of all authors. All authors have given approval to the final version of the manuscript.

Funding

This work was partially funded by the National Science Foundation, under Award Number NSF ECCS-1650002.

Notes

The authors declare no competing financial interest.

REFERENCES

(1) Sannicolo, T.; Lagrange, M.; Cabos, A.; Celle, C.; Simonato, J.-P.; Bellet, D. Metallic Nanowire-Based Transparent Electrodes for Next Generation Flexible Devices: a Review. *Small* **2016**, *12*, 6052−6075.

(2) Liu, Z.; Xu, J.; Chen, D.; Shen, G. Flexible electronics based on inorganic nanowires. *Chem. Soc. Rev.* **2015**, *44*, 161−192.

(3) Kou, P.; Yang, L.; Chang, C.; He, S. Improved Flexible Transparent Conductive Electrodes based on Silver Nanowire Networks by a Simple Sunlight Illumination Approach. *Sci. Rep.* **2017**, *7*, 42052.

(4) Ellmer, K. Past achievements and future challenges in the development of optically transparent electrodes. *Nat. Photonics* **2012**, *6*, 809−817.

(5) Kim, S. J.; Kang, J.-H.; Mutlu, M.; Park, J.; Park, W.; Goodson, K. E.; Sinclair, R.; Fan, S.; Kik, P. G.; Brongersma, M. L. Anti-

Hermitian photodetector facilitating efficient subwavelength photon sorting. *Nat. Commun.* **2018**, *9*, 316.
(6) Garnett, E. C.; Cai, W.; Cha, J. J.; Mahmood, F.; Connor, S. T.; Greyson Christoforo, M.; Cui, Y.; McGehee, M. D.; Brongersma, M. L. Self-limited plasmonic welding of silver nanowire junctions. *Nat. Mater.* **2012**, *11*, 241−249.
(7) Ferry, V. E.; Munday, J. N.; Atwater, H. A. Design Considerations for Plasmonic Photovoltaics. *Adv. Mater.* **2010**, *22*, 4794−4808.
(8) van de Groep, J.; Spinelli, P.; Polman, A. Transparent Conducting Silver Nanowire Networks. *Nano Lett.* **2012**, *12*, 3138−3144.
(9) Ferry, V. E.; Sweatlock, L. A.; Pacifici, D.; Atwater, H. A. Plasmonic Nanostructure Design for Efficient Light Coupling into Solar Cells. *Nano Lett.* **2008**, *8*, 4391−4397.
(10) Hu, L.; Kim, H. S.; Lee, J.-Y.; Peumans, P.; Cui, Y. Scalable Coating and Properties of Transparent, Flexible, Silver Nanowire Electrodes. *ACS Nano* **2010**, *4*, 2955−2963.
(11) Atwater, H. A.; Polman, A. Plasmonics for improved photovoltaic devices. *Nat. Mater.* **2010**, *9*, 205−213.
(12) Ferry, V. E.; Verschuuren, M. A.; Li, H. B. T.; Verhagen, E.; Walters, R. J.; Schropp, R. E. I.; Atwater, H. A.; Polman, A. Light trapping in ultrathin plasmonic solar cells. *Opt. Express* **2010**, *18*, A237−A245.
(13) Kuang, P.; Park, J.-M.; Liu, G.; Ye, Z.; Leung, W.; Chaudhary, S.; Lynch, D.; Ho, K.-M.; Constant, K. Metal-nanowall grating transparent electrodes: Achieving high optical transmittance at high incident angles with minimal diffraction. *Opt. Express* **2013**, *21*, 2393−2401.
(14) Blakers, A. W. Shading losses of solar-cell metal grids. *J. Appl. Phys.* **1992**, *71*, 5237−5241.
(15) Chen, F.-h.; Pathreeker, S.; Kaur, J.; Hosein, I. D. Increasing light capture in silicon solar cells with encapsulants incorporating air prisms to reduce metallic contact losses. *Opt. Express* **2016**, *24*, A1419−A1430.
(16) Munday, J. N.; Atwater, H. A. Large Integrated Absorption Enhancement in Plasmonic Solar Cells by Combining Metallic Gratings and Antireflection Coatings. *Nano Lett.* **2011**, *11*, 2195−2201.
(17) Lossen, J.; Rudolph, D.; Koduvelikulathu, L. J.; Carvalho, R.; Rossetto, M. P.; Borsato, O.; Bortoletto, E.; Galiazzo, M. Double Printing nPERT Cells with Narrow Contact Layers. *Energy Procedia* **2016**, *92*, 939−948.
(18) Saive, R.; Atwater, H. A. Mesoscale trumps nanoscale: metallic mesoscale contact morphology for improved light trapping, optical absorption and grid conductance in silicon solar cells. *Opt. Express* **2018**, *26*, A275−A282.
(19) Ward, J. S.; Duda, A.; Friedman, D. J.; Geisz, J.; McMahon, W.; Young, M. High aspect ratio electrodeposited Ni/Au contacts for GaAs-based III−V concentrator solar cells. *Prog. Photovoltaics* **2015**, *23*, 646−653.
(20) Saive, R.; Borsuk, A. M.; Emmer, H. S.; Bukowsky, C. R.; Lloyd, J. V.; Yalamanchili, S.; Atwater, H. A. Effectively Transparent Front Contacts for Optoelectronic Devices. *Adv. Opt. Mater.* **2016**, *4*, 1470−1474.
(21) Stephens, R. B.; Cody, G. D. Optical reflectance and transmission of a textured surface. *Thin Solid Films* **1977**, *45*, 19−29.
(22) Southwell, W. H. Pyramid-array surface-relief structures producing antireflection index matching on optical surfaces. *J. Opt. Soc. Am. A* **1991**, *8*, 549−553.
(23) Dobrowolski, J. A.; Poitras, D.; Ma, P.; Vakil, H.; Acree, M. Toward perfect antireflection coatings: numerical investigation. *Appl. Opt.* **2002**, *41*, 3075−3083.
(24) Yan, X.; Poxson, D. J.; Cho, J.; Welser, R. E.; Sood, A. K.; Kim, J. K.; Schubert, E. F. Enhanced Omnidirectional Photovoltaic Performance of Solar Cells Using Multiple-Discrete-Layer Tailored- and Low-Refractive Index Anti-Reflection Coatings. *Adv. Funct. Mater.* **2013**, *23*, 583−590.
(25) Hsu, P.-C.; Wang, S.; Wu, H.; Narasimhan, V. K.; Kong, D.; Ryoung Lee, H.; Cui, Y. Performance enhancement of metal nanowire transparent conducting electrodes by mesoscale metal wires. *Nat. Commun.* **2013**, *4*, 2522.
(26) Kik, P. G. Catoptric electrodes: transparent metal electrodes using shaped surfaces. *Opt. Lett.* **2014**, *39*, 5114−5117.
(27) Sun, M.; Kik, P. G. Scale dependent performance of metallic light-trapping transparent electrodes. *Opt. Express* **2020**, *28*, 18112−18121.
(28) Sun, M.; Kik, P. G. Light trapping transparent electrodes with a wide-angle response. *Opt. Express* **2021**, *29*, 24989−24999.
(29) CST Microwave Studio. https://www.3ds.com/products-services/simulia/products/cst-studio-suite/?utm_source=cst.com&utm_medium=301&utm_campaign=cst (accessed Sep 18, 2021).
(30) Johnson, P. B.; Christy, R. W. Optical Constants of the Noble Metals. *Phys. Rev. B: Solid State* **1972**, *6*, 4370−4379.
(31) Hidber, P. C.; Helbig, W.; Kim, E.; Whitesides, G. M. Microcontact Printing of Palladium Colloids: Micron-Scale Patterning by Electroless Deposition of Copper. *Langmuir* **1996**, *12*, 1375−1380.
(32) Farrer, R. A.; LaFratta, C. N.; Li, L.; Praino, J.; Naughton, M. J.; Saleh, B. E.; Teich, M. C.; Fourkas, J. T. Selective functionalization of 3-D polymer microstructures. *J. Am. Chem. Soc.* **2006**, *128*, 1796−1797.
(33) Tal, A.; Chen, Y.-S.; Williams, H. E.; Rumpf, R. C.; Kuebler, S. M. Fabrication and characterization of three-dimensional copper metallodielectric photonic crystals. *Opt. Express* **2007**, *15*, 18283−18293.
(34) Johnson, B. C. Electrical resistivity of copper and nickel thin-film interconnections. *J. Appl. Phys.* **1990**, *67*, 3018−3024.
(35) Cui, X.; Hutt, D. A.; Conway, P. P. Evolution of microstructure and electrical conductivity of electroless copper deposits on a glass substrate. *Thin Solid Films* **2012**, *520*, 6095−6099.
(36) Bass, J.; Dugdale, J.; Foiles, C. *Landolt-Bvrnstein: Numerical Data and Functional Relationships in Science and Technology—New Series Gruppe/Group 3 Condensed Matter Volume 15 Metals: Electronic Transport Phenomena/Metalle: Elektronische Transportphdnomene*; Springer-Verlag, 1982.
(37) Steinhögl, W.; Schindler, G.; Steinlesberger, G.; Traving, M.; Engelhardt, M. Comprehensive study of the resistivity of copper wires with lateral dimensions of 100 nm and smaller. *J. Appl. Phys.* **2005**, *97*, 023706.
(38) Xia, C.; Gutierrez, J. J.; Kuebler, S. M.; Rumpf, R. C.; Touma, J. Cylindrical-lens-embedded photonic crystal based on self-collimation. *Opt. Express* **2022**, *30*, 9165−9180.
(39) Golvari, P.; Kuebler, S. M. Fabrication of Functional Microdevices in SU-8 by Multi-Photon Lithography. *Micromachines* **2021**, *12*, 472.
(40) Ordouie, E.; Alisafaee, H.; Siahmakoun, A. Ultracompact polarizing beam splitter based on single-material birefringent photonic crystal. *Opt. Lett.* **2018**, *43*, 4288−4291.
(41) Barranco, A.; Borras, A.; Gonzalez-Elipe, A. R.; Palmero, A. Perspectives on oblique angle deposition of thin films: From fundamentals to devices. *Prog. Mater. Sci.* **2016**, *76*, 59−153.
(42) Clukay, C. J.; Grabill, C. N.; Hettinger, M. A.; Dutta, A.; Freppon, D. J.; Robledo, A.; Heinrich, H.; Bhattacharya, A.; Kuebler, S. M. Controlling formation of gold nanoparticles generated in situ at a polymeric surface. *Appl. Surf. Sci.* **2014**, *292*, 128−136.

https://doi.org/10.1021/acsphotonics.2c01468
ACS Photonics XXXX, XXX, XXX−XXX